ASSESSMENT OF RANS AT LOW PRANDTL NUMBER AND SIMULATION OF SODIUM BOILING FLOWS WITH A CMFD CODE

S. Mimouni[1], C. Baudry[1], M. Guingo[1], M. Hassanaly[1], V. Heisel[2], J. Lavieville[1], N. Mechitoua[1], N. Mérigoux[1].

[1]: Electricité de France, R&D Division, 6 Quai Watier, 78401 Chatou, France

[2]: ENSEEIT, 2 rue Charles Camichel, 31000 Toulouse, France

Stephane.mimouni@edf.fr

ABSTRACT

In France, Sodium-cooled Fast Reactors (SFR) have recently received a renewed interest. In 2006, the decision was taken by the French Government to initiate research in order to build a first Generation IV prototype (called ASTRID) by 2020. The improvement in the safety of SFR is one of the key points in their conception.

Accidental sequences may lead to a significant increase of reactivity. This is for instance the case when the sodium coolant is boiling within the fissile zone. As a consequence, incipient boiling superheat of sodium is an important parameter, as it can influence boiling process which may appear during some postulated accidents as the unprotected loss of flow (ULOF). The problem is that when boiling conditions are reached, the flow decreases progressively and vapour expands into the heating zone. A crucial investigating way is to optimize the design of the fissile assemblies of the core in order to lead to stable boiling during a ULOF accident, without voiding of the fissile zone.

Moreover, in order to evaluate nuclear plant design and safety, a CFD tool has been developed at EDF in the framework of the nuclear industry. Advanced models dedicated to boiling flows have been implemented and validated against experimental data for ten years now including a wall law for boiling flows, wall transfer for nucleate boiling, turbulence and polydispersion model. This paper aims at evaluating the generalization of these models to SFR. At least two main issues are encountered:

- Firstly, at low Prandtl numbers such as those of liquid metal, classical approaches derived for unity or close to unity fail to accurately predict the heat transfer. In order to evaluate the wall law implemented in the CFD tool, computations have been compared with KALLA experimental results obtained in the case of a rod heated with a constant heat flux which is concentrically embedded in a pipe liquid metal flow (single-phase flow).
- Secondly, the incipient boiling superheat of sodium is quite different from that of conventional fluids. As a consequence, the nucleate boiling model has been improved and validated against the Charlety's experiment where a rod heated with a constant heat flux is concentrically embedded in a pipe sodium flow. For different values of the heat flux, the pressure is measured at different locations as function of the mass flow rate. A reasonable agreement has been reached which is very encouraging for further applications.

Finally, preliminary computations have been carried out in an assembly constituted of 19 pins equipped with a wrapped wire where partial experimental results are available. Computations have shown a pressure drop at the end of the heated length due to the sudden increase of the hydraulic diameter. Thus, the pressure can drop below the vapour pressure leading to liquid vaporization. This first result supports the assumption of boiling in the upper subassembly zone which could possibly lead to a sodium boiling stabilization.

KEYWORDS

Boiling flow, SFD, sodium, low Prandtl number, SFR assembly.

1. INTRODUCTION

Extended sodium boiling in the fissile zone of a fast breeder reactor (FBR) implies a risk of transient over-power (TOP) and subsequent core melting. Extended sodium boiling may be a consequence of an unprotected loss of flow accident (ULOF).

Seiler et al. have proposed a mitigation strategy [1], based on boiling stabilisation. This approach is based on the LEDINEGG criterion. If the stability criterion is not satisfied a flow excursion will develop (called static instability or LEDINEGG instability): the flow will decrease progressively, and vapour will expand into the heating zone. A new stable working point (high quality boiling) may theoretically be reached where the stability criterion is again satisfied. The model has been adapted to the description of the pressure variation at boiling onset (i.e. for low quality boiling). The model calculates the void fraction distribution and related gravity and friction pressure drops in the bundle. A homogeneous 1-D two-phase flow model approach is used in [1] and the pressure drop is calculated by making use of the Lockhart–Martinelli model approach.

The main objective of this paper is to generalize this one-dimensional approach by making use of CFD tool. Indeed, we compute the void fraction by a 3D two-fluid two-phase flow model .

Firstly, the models implemented in the CFD tool are described. In section 4, computations are compared with KALLA experimental results obtained in the case of a rod heated with a constant heat flux which is concentrically embedded in a pipe liquid metal flow (single-phase flow). In section 5, computations are performed in the Charlety's experiment geometry where a rod heated with a constant heat flux is concentrically embedded in a pipe sodium flow (boiling flow). The last section presents preliminary computations in an assembly constituted of 19 pins equipped with a wrapped wire.

2. THE NEPTUNE_CFD SOLVER AND PHYSICAL MODELLING

2.1 Introduction

NEPTUNE_CFD is a three dimensional two-fluid code developed more especially for nuclear reactor applications. This local three-dimensional module is based on the classical two-fluid one pressure approach, including mass, momentum and energy balances for each phase.

The NEPTUNE_CFD solver, based on a pressure correction approach, is able to simulate multi-component multiphase flows by solving a set of three balance equations for each field (fluid component and/or phase) . These fields can represent many kinds of multiphase flows: distinct physical components (e.g. gas, liquid and solid particles); thermodynamic phases of the same component (e.g.: liquid water and its vapour); distinct physical components, some of which split into different groups (e.g.: water and several groups of different diameter bubbles); different forms of the same physical components (e.g.: a continuous liquid field, a dispersed liquid field, a continuous vapour field, a dispersed vapour field). The solver is based on a finite volume discretization, together with a collocated arrangement for all variables. The data structure is totally face-based, which allows the use of arbitrary shaped cells (tetraedra, hexahedra, prisms, pyramids ...) including non conforming meshes [2].

2.2 Governing equations and physical modelling

The CFD module of the NEPTUNE software platform [3] based on the two-fluid approach [4]. In this approach, a set of local balance equations for mass, momentum and energy is written for each phase. These balance equations are obtained by ensemble averaging of the local instantaneous balance equations written for the two phases. When the averaging operation is performed, the major part of the information about the interfacial configuration and the microphysics governing the different types of exchanges is lost. As a consequence, a number of closure relations (also called constitutive relations) must be supplied for the total number of equations (the balance equations and the closure relations) to be equal to the

number of unknown fields. We can distinguish three different types of closure relations: those which express the inter-phase exchanges (interfacial transfer terms), those which express the intra-phase exchanges (molecular and turbulent transfer terms) and those which express the interactions between each phase and the walls (wall transfer terms). The balance equations of the two-fluid model we use for two-phase boiling flows and their closure relations are described in the following subsections.

Main set of balance equations

The two-fluid model we use for our two-phase boiling flow computations consists of the following balance equations.

Two mass balance equations:

$$\frac{\partial \alpha_k \rho_k}{\partial t} + \nabla.\left(\alpha_k \rho_k \underline{V}_k\right) = \Gamma_k \qquad k = l, v \tag{1}$$

where t is the time, α_k, ρ_k, $\underline{V}_k$ denote the fraction of phase k, its averaged density and velocity. The phase index k takes the values l for the liquid phase and v for vapour bubbles.

Two momentum balance equations:

$$\frac{\partial \alpha_k \rho_k \underline{V}_k}{\partial t} + \nabla.\left(\alpha_k \rho_k \underline{V}_k \underline{V}_k\right) = -\alpha_k \nabla p + \underline{M}_k + \Gamma_k \underline{V}_k + \alpha_k \rho_k \underline{g} + \nabla.\left[\alpha_k \left(\underline{\underline{\Sigma}}_k + \underline{\underline{R}}_k\right)\right] \quad k = l, v, \tag{2}$$

where p is the pressure, $\underline{g}$ is the gravity acceleration, $\underline{M}_k$ is the interfacial momentum transfer per unit volume and unit time, and $\underline{\underline{\Sigma}}_k$ and $\underline{\underline{R}}_k$ denote the molecular and turbulent stress tensors, the latter being also called the Reynolds stress tensor. The wall friction terms for the two phases do not appear in the momentum balance equations because solid walls are only present at the boundaries of the flow domain and the wall friction is expressed through the wall boundary conditions.

Two total enthalpy balance equations:

$$\frac{\partial}{\partial t}\left[\alpha_k \rho_k \left(h_k + \frac{V_k^{\,2}}{2}\right)\right] + \nabla.\left(\alpha_k \rho_k \left(h_k + \frac{V_k^{\,2}}{2}\right)\underline{V}_k\right) = \alpha_k \frac{\partial p}{\partial t} + \alpha_k \rho_k \underline{g}.\underline{V}_k + \Gamma_k \left(h_{ki} + \frac{V_k^{\,2}}{2}\right) \tag{3}$$
$$+ \Pi_k^{'} A_i + q_{wk}''' - \nabla.\left[\alpha_k \left(\underline{q}_k + \underline{q}_k^{\,T}\right)\right] \qquad k = l, v$$

where h_k is the phase-averaged enthalpy for phase k and h_{ki} is the interfacial-averaged enthalpy. We have assumed that the two phases are governed by the same averaged pressure field p and we make no distinction between the pressures in the two phases or between the bulk pressure and the interface pressure for simplicity. The three terms Γ_k, $\underline{M}_k$ and $\Pi_k^{'} A_i$ denote the interfacial transfer terms of mass, momentum and heat, the quantity A_i being the interfacial area concentration. The term q_{wk}''' denotes the wall-to-fluid heat transfer per unit volume and unit time for each phase. The two terms $\underline{q}_k$ and $\underline{q}_k^{\,T}$ denote the molecular and turbulent heat fluxes inside phase k. The work of viscous stresses of momentum is neglected in the enthalpy equation.

The interfacial transfer of momentum $\underline{M}_k$ appearing in the RHS of Eq. (2) is assumed to be the sum of four forces:

$$\underline{M}_k = \underline{M}_k^{\,D} + \underline{M}_k^{\,AM} + \underline{M}_k^{\,L} + \underline{M}_k^{\,TD} \tag{4}$$

The four terms are the averaged drag, added mass, lift and turbulent dispersion forces per unit volume.

The turbulent transfer terms for the liquid phase are calculated by using the Reynolds Stress Transport Model SSG [5-6-7].

Interfacial transfer terms

If the mechanical terms are neglected in comparison to the thermal terms in the averaged form of the energy jump condition, this condition reduces to:

$$\sum_k \left(\Gamma_k h_{ki} + q''_{ki} A_i\right) \approx 0 . \tag{5}$$

This important relation (together with the mass jump condition $\Gamma_l = -\Gamma$) allows to compute the mass transfer terms as functions of the interfacial heat transfer terms $q''_{ki} A_i$ and the interfacial-averaged enthalpies h_{ki} :

$$\Gamma_l = -\Gamma_v = \frac{q''_{li} + q''_{vi}}{h_{vi} - h_{li}} A_i . \tag{6}$$

We have no information about the dependence of the interfacial- averaged enthalpies h_{ki}. Therefore, two basic assumptions can be made: (1) the interfacial-averaged enthalpies h_{ki} are identified to the phase-averaged ones h_k or (2) the interfacial-averaged enthalpies h_{ki} are given by the saturation enthalpies. Here we have made the assumption (1). Each interfacial heat transfer term $q''_{ki} A_i$ is the product of the interfacial heat flux density:

$$q''_{ki} = C_{ki}\left(T_{sat}(p) - T_k\right), \tag{7}$$

where C_{ki}, T_k and $T_{sat}(p)$ denote a heat transfer coefficient, the averaged temperature of phase k and the saturation temperature. The interfacial area concentration is expressed as $A_i = 6\alpha / d$, where α is the void fraction and d is the mean bubble diameter. The following heat transfer coefficient is used:

$$C_{li} = \frac{Nu_l k_l}{d} \quad Nu_l = 2 + 0.6\,\mathrm{Re}^{1/2}\,\mathrm{Pr}_l^{1/3} \quad \mathrm{Re}_b \triangleq \frac{\left|\underline{V}_v - \underline{V}_l\right| d}{\nu_l} \quad \mathrm{Pr}_l \triangleq \frac{\nu_l}{a_l}, \tag{8}$$

where Re_b is the bubble Reynolds number and Pr_l is the liquid Prandtl number, ν_l being the liquid kinematic viscosity. The heat transfer coefficient between the vapour and the interface for the case of bubbles is written as:

$$C_{vi} A_i = \frac{\alpha \rho_v C_{pv}}{t_c}, \tag{9}$$

where C_{pv} is the gas heat capacity at constant pressure and t_c is a characteristic time given by the users. This relation simply ensures that the vapour temperature T_v remains very close to the saturation temperature T_{sat}, which is the expected result for bubbly flows with sufficiently small bubbles (flow in a PWR core in conditions close to nominal).

Wall transfer model for nucleate boiling

In a first simplified approach, and following the analysis of Kurul at al. [9], the boiling heat flux is split into three terms:

- a single phase flow convective heat flux q_c at the fraction of the wall area unaffected by the presence of bubbles,
- a quenching heat flux q_q where bubbles departure bring cold liquid in contact with the wall periodically,
- a vaporisation heat flux q_e needed to generate the vapour phase.

Each of these three phenomena is expressed by a heat flux density (per unit surface of the heated wall) which is related to the volumetric heat flux by the following relation:

$$q'''_{wl} = \frac{A_w}{V} q''_{wl} = \frac{A_w}{V}\left(q_c + q_q + q_e\right), \tag{10}$$

where A_w is the heated wall surface in contact to the cell having volume V, therefore q'''_{wl} is expressed in W/m^3 and q''_{wl} as well as q_c, q_q and q_e are expressed in W/m^2. The quantities q_c, q_q and q_e denote the heat flux densities due to liquid convective heat transfer, quenching and evaporation respectively. The liquid convective heat transfer per unit surface of the heated wall is written as:

$$q_c = A_c h_{\log}(T_w - T_l), \tag{11}$$

where T_w is the wall temperature and h_{log} is a heat exchange coefficient which is given by:

$$h_{\log} = \rho_l C_{pl} \frac{u^*}{T^+}, \tag{12}$$

where u^* is the wall friction velocity and T^+ is the non-dimensional liquid temperature. The velocity u^* is calculated from the logarithmic law of the wall written for the liquid velocity in the wall boundary layer. The non-dimensional temperature follows a similar logarithmic profile.

The heat flux density due to quenching is written as:

$$q_q = A_b t_q f \frac{2\lambda_l (T_w - T_l)}{\sqrt{\pi a_l t_q}}, \tag{13}$$

where A_b is the wall fraction occupied by bubble nucleation, f is the bubble detachment frequency, t_q is the quenching time and a_l is the liquid thermal diffusivity. The two fractions A_c and A_b are given by:

$$\begin{aligned} A_b &= \min\left(1, n\pi d_d^{\,2}/4\right), \\ A_c &= 1 - A_b \end{aligned} \tag{14}$$

where n is the active nucleation sites density (per unit surface of the heated wall) and d_d is the bubble detachment diameter. The active nucleation sites density is modelled according to Kurul et al. [9]:

$$n = \left[210(T_w - T_{sat})\right]^{1.8}, \tag{15}$$

as a function of the wall superheating. The bubble detachment diameter is given by the correlation from Unal et al. [12]. The Unal's correlation is valid for subcooled liquid but has been extended to saturated liquid. The bubble detachment diameter is given by:

$$d_d = 2.4210^{-5} p^{0.709} \frac{a}{\sqrt{b\varphi}}, \tag{16}$$

where p is the pressure and a, b and φ are given by the following relations:

$$a = \frac{(T_w - T_{sat})\lambda_s}{2\rho_v \ell \sqrt{\pi a_s}}, \tag{17}$$

where λ_s and a_s denote the wall conductivity and thermal diffusivity, ρ_v denotes the vapour density and ℓ is the latent heat of vaporisation. In the modified correlation, b is given by:

$$b = \begin{cases} \dfrac{(T_{sat} - T_l)}{2(1 - \rho_v/\rho_l)} & St < 0.0065 \\ \dfrac{1}{2(1-\rho_v/\rho_l)} \dfrac{q_c + q_q + q_e}{0.0065 \rho_l C_{pl} \|V_l\|} & St > 0.0065 \end{cases}, \tag{18}$$

where $\|V_l\|$ is the norm of the liquid velocity and St is the Stanton number which is defined by:

$$St \hat{=} \frac{q_c + q_q + q_e}{\rho_l C_{pl} \|V_l\| (T_{sat} - T_l)}, \quad (19)$$

and the quantity φ appearing in Eq. (23) is given by :

$$\varphi = \max\left(1, \left(\frac{\|V_l\|}{V_0}\right)^{0.47}\right) \qquad V_0 = 0.61 m/s, \quad (20)$$

The quenching time and the bubble detachment frequency are modelled as:

$$t_q = 1/f \qquad f = \sqrt{\frac{4}{3}\frac{g|\rho_v - \rho_l|}{\rho_l d_d}}, \quad (21)$$

The third heat flux density q_e used for evaporation is given by:

$$q_e = f \frac{\pi d_d^{\,3}}{6} \rho_v \ell n .$$

The superheat of the liquid (dedicated to the sodium) is taken into account by:

$\Delta P = Pv - PI = 2\sigma/r_B$, which gives $\Delta T_{sat} = Tv - T_{sat} = \Delta P \frac{T_{sat}}{l\rho_v} = \frac{2\sigma}{r_B}\frac{T_{sat}}{l\rho_v}$, where Pv is the pressure inside a bubble of radius r_B.

Wall function for boiling flow

In subcooled flow boiling, the liquid velocity profile in the boundary layer is significantly disturbed by the bubble formation and detachment mechanisms on the heated wall. In the literature, an over-prediction of liquid and gas velocity distributions in the boiling boundary region has been reported. The use of single-phase wall law may be one of the main reasons for these results. Following Ramstorfer et al. [13], Mimouni et al. [6] suggested a wall function for boiling flows. When the void fraction tends to zero, the wall law tends to the single-phase formulation. Furthermore, this relation depends on bubble diameter and bubble density at the wall (void fraction at the wall), which is physically expected.

By using the Van Driest formulation :

$$u^+ = \int_0^{y^+} \frac{2d\xi}{1 + \sqrt{1 + 4\kappa^2(1 - \exp(-\xi/A))^2\xi^2}} - \Delta u^+$$

Where Δu^+ is due to the roughness induced by bubbles created at the wall :

$$\Delta u^+ = \begin{cases} 0; & k_r^+ \le 11.3 \\ \frac{1}{\kappa}\ln(1 + C_{kr} k_r^+); & k_r^+ > 11.3 \end{cases}$$

with $C_{kr} = 0.5$ and k_r^+ (similar to a Reynolds number) expressed as :

$k_r^+ = \frac{\rho_l k_r \sqrt{u_w u^*}}{\mu_l}$, where $u^* = c_\mu^{1/4} k_l^{1/2}$, u_w the friction velocity and $k_r = \alpha_v D$.

3. VALIDATION FOR ADIABATIC BUBBLY FLOWS AND BOILING FLOWS

Since the maturity of two-phase CFD has not reached yet the same level as single phase CFD, an important work of model development and thorough validation is needed. Many of these applications involve bubbly and water boiling flows, and therefore it is essential to validate the software on such configurations. Four experiments were selected for the validation. The Liu and Bankoff experiment (1993) is an adiabatic air-water bubbly flow inside a vertical pipe. It allows to validate forces applied to

the bubbles. The Bel F'Dhila and Simonin (1992) experiment is an adiabatic bubbly air-water flow inside a sudden pipe expansion. It allows to validate the dynamic models and turbulence. The DEBORA and the ASU facilities provide results for boiling flows inside a vertical pipe. The working fluid is refrigerant R12 for DEBORA and R113 for ASU. Both allow to validate the nucleation modeling on a heated wall, and ASU allows also the validation of the two-phase wall function. A key feature of this work is that all these computations were performed with a single and consistent set of models. Douce et al. [14] have shown that the physical models implemented in NEPTUNE_CFD have captured experimental profiles with reasonable accuracy.

4. HEATED ROD IN A VERTICAL ANNULUS

For linear eddy viscosity models, we can define the turbulent Prandtl number Prt as the ratio of the turbulent viscosity to turbulent thermal diffusivity analogous to the molecular Prandtl number. In the following, the turbulent terms are calculated by using the $R_{ij} - \epsilon$ SSG model. But, the closure law for the turbulent heat flux is the same as the one used for linear eddy viscosity models. Moreover, the turbulent Prandtl number is assumed to be a constant. Modeling the turbulent heat fluxes by introducing Prt as constant can result in a significant inaccuracy related to the transferred heat in the case of turbulent flows of low Prandtl number. But, the objective of this section is to evaluate the discrepancies in a single phase flow of turbulent flows of low Prandtl number. The final objective concerns sodium boiling flows (low Prandtl number) and the experience gained over several decades in boiling flows shows that crucial phenomena in single phase flow is likely to become of second order compared to others crucial phenomena occurring in boiling flows.

Figure 1 displays the experimental setup of a generic experiment conducted in KALLA [15]. Hereby, a rod heated with a constant heat flux is concentrically embedded in a pipe flow. More details on the experimental set-up may be taken from [15].
Regarding the inlet condition, an isothermal turbulent hydraulically fully developed pipe flow with a radius R0=0.03 m.

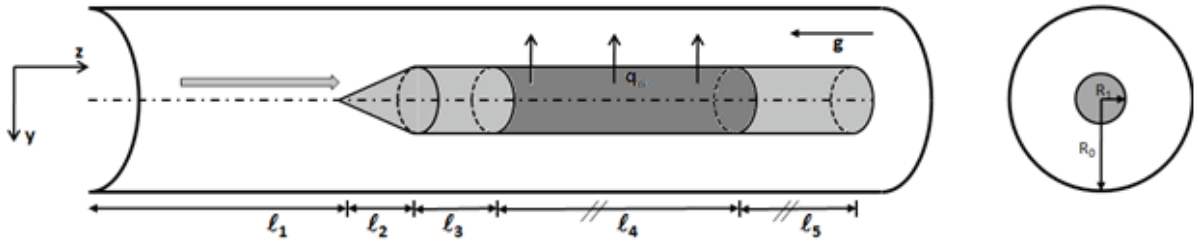

Figure 1: Schematic diagram of the geometric setup of the heated rod simulations

The rod is uniformly heated with Q= 3kW ($q_w = Q/(2l_4\pi R_i)$ kW/m^2) at position z*=0 with $z^*=z/2R_i$ along l_4. It is followed by an unheated zone, which has been chosen in the numerical simulations to a length l_6. The different lengths are given in table I.

Table I. Separate effect and integral

l_1	l_2	l_3	l_4	l_5
0.35m	0.0216m	0.028m	0.86m	0.34m

The Reynolds number of the investigated case is $Re_{D_h} = 59100$ ($v_{inlet} = 0.52$ m/s). The inlet temperature is $T_{inlet} = 424$ K. The flow is assumed to be axi-symmetric therefore a two-dimensional axi-symmetric meshing is used. The thermophysical properties of the fluid are given in table II [14].

Table II. Thermophysical properties of the fluid		
Density	$\boldsymbol{\rho = 11.113 - 1.75 \cdot 10^{-3} T}$	$\boldsymbol{10^3\ kg/m^3}$
Viscosity	$\mu = 0.497\exp(741/T)$	$10^{-3}\ Pa \cdot s$
Thermal conductivity	$\lambda = 6.851 + 10.147 \cdot 10^{-3} T$	$W/(mK)$
Heat capacity	$c_p = 0.16 - 2.385 \cdot 10^{-5} T$	$10^3\ J/(kg\ K)$

Figure 2 and Figure 3 represent the velocity profiles and the temperature profiles along the y-direction at different locations z*. A reasonable agreement is obtained for the velocity profiles but the liquid temperature is over-estimated near the wall with Neptune_CFD. As a consequence, for industrial applications, Neptune_CFD overestimates the occurrence of the case when the sodium coolant is boiling within the fissile zone. In others words, this overestimation is favourable for safety. Nevertheless, the modelling of the turbulent heat flux should be improved in further computations in order to reduce safety margins.

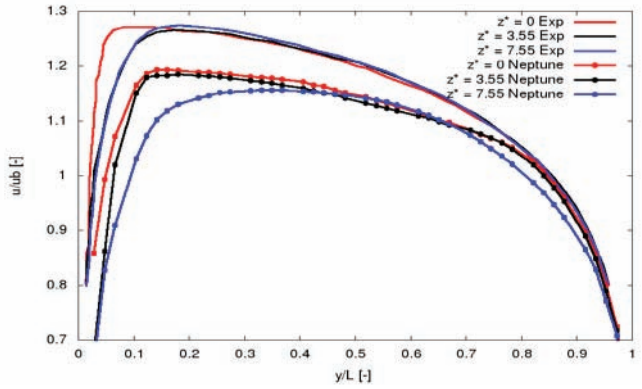

Figure 2: Comparison of the velocity profiles as function of y/L for Re = 59100

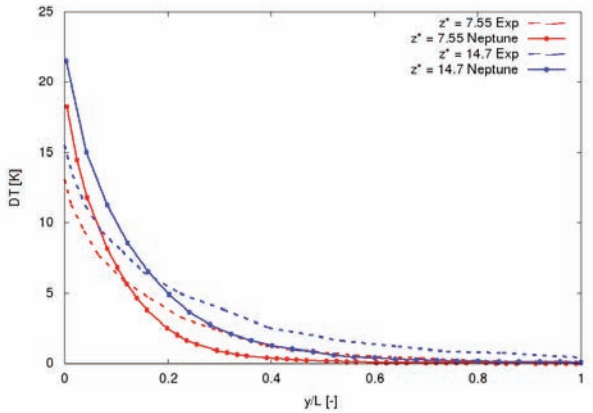

Figure 3: Comparison of the temperature profiles at position z* = 7.55 and z* = 14.7 over y/L

5. CHARLETY'S EXPERIMENT

Sodium boiling tests in forced convection has been carried out by Charlety et al (1970) 45 years ago at CEA [17]. The test section was a heating pin of 6.6 mm, 600 mm long inside a tube of 8.6 mm followed by a non heated length of 6 mm and 450 mm long and 4 mm (Figure 4).

The parameter range was in order to simulate the Phenix reactor pressure distribution regarding heat flux (between 80 and 200 W/cm2), outlet pressure (1.2 bar), mass flowrate (from 10-4 kg/s to 1.6.10-6 kg/s),and inlet temperature (450°C). The flow is assumed to be axi-symmetric therefore a two-dimensional axi-symmetric meshing is used.

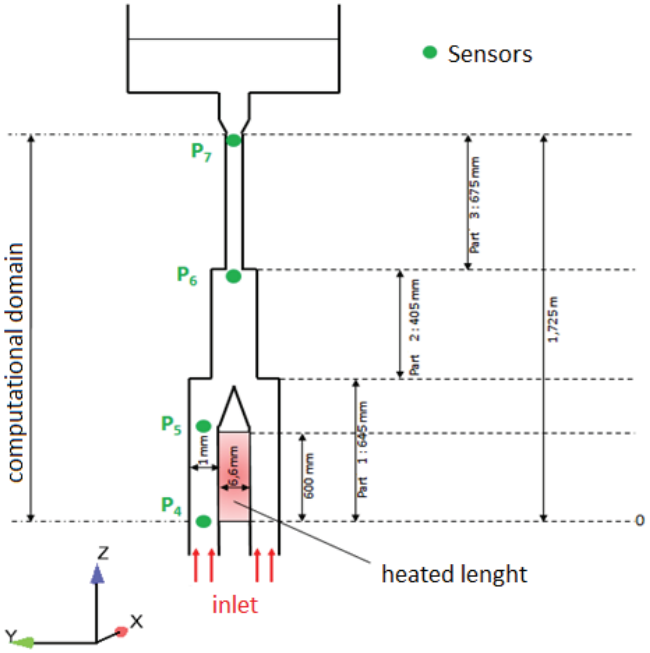

Figure 4: : General view of the experiment; pressure measurements are located in P4, P5, P6 and P7

The objective of this section is to compare the measured values and the simulated values for the internal characteristic. The internal characteristic is the variation of pressure drop over the channel induced by single and/or two-phase flow when the inlet flow rate is varied under constant power, constant outlet pressure, and constant inlet temperature. For a low pressure sodium flow, the shape of the internal characteristic affects the form of a S-curve, due to the physical properties of sodium [1].

In single phase flow (large values of mass flow rate) pressure drops exhibit an increase when the mass flow rate increases (frictional pressure drops increase whereas gravitational pressure drops are negligible). In boiling regime (low values of the mass flow rate), gravitational pressure drops decrease (because of the density) whereas frictional pressure drops increase (conservation of the mass flow rate). The boiling onset point corresponds to the minimum of the S-curve.

In good agreement with the behaviour described above, Figure 6 and Figure 7 represent the internal characteristic of the test section for two values of the heat flux of the heating pin. Experimental values and numerical results are in reasonable accordance. Moreover, the prediction of the boiling onset is particularly encouraging.

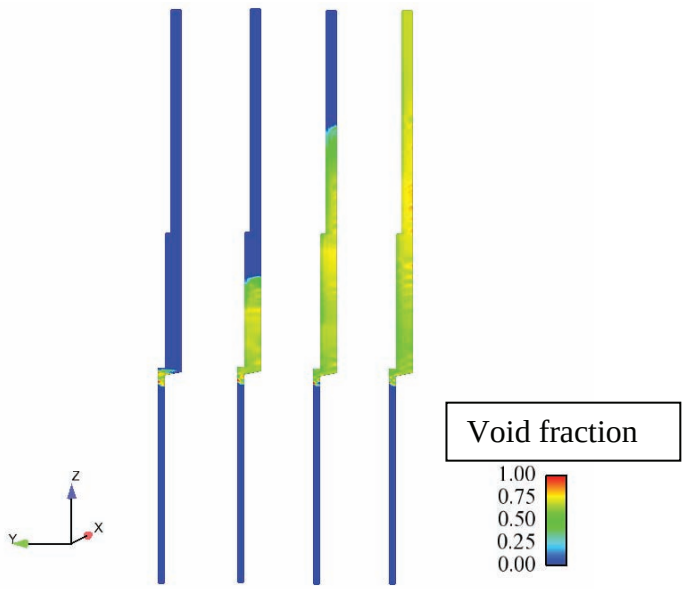

Figure 5: Evolution of the void fraction in the computational domain.

Figure 5 represent the evolution of the void fraction. It is of relevance interest to see that ebullition occurs at the end of the heated length. The pressure drops below the vapour pressure leading to liquid vaporization. As a consequence, the main phenomenon is mainly due to the autovaporisation of sodium instead of ebullition in cells adjacent to the heated length.

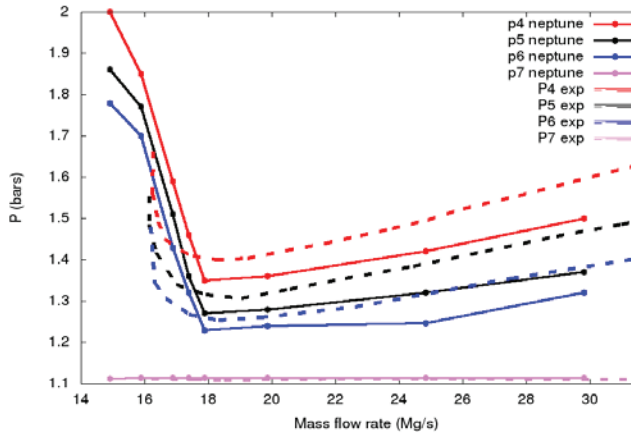

Figure 6: Pressure profiles vs mass flow rate at inlet. Case Q=10kW.

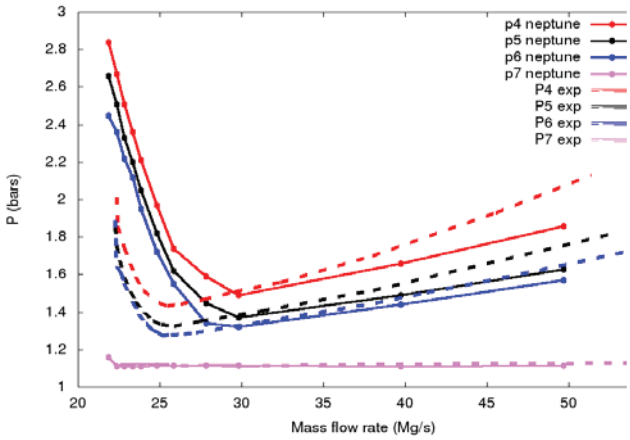

Figure 7: Pressure profiles vs mass flow rate at inlet. Case Q=15kW.

6. 19 HEATING PIN BUNDLE

A reasonable agreement has been obtained on sodium boiling in single channel configuration in the previous section. It is now interesting to go further and to assess the capabilities of the CFD tool for test sections more representative of fast reactor sub-assemblies. Working to this end, the GR19 19 heating pin bundle has been developed at CEA [19]. Figure 8, Figure 9 and Figure 10 give a view of the complexity of the geometry simulated with Neptune_CFD. In this section, Neptune_CFD is coupled with SYRTHES code in order to deal with heat transfer at the fluid/solid interface. The thermal code SYRTHES

developed at EDF solves the energy conservation in a solid from the distribution of heat in a pin [18].

The liquid velocity at inlet is 5 m/s. The inlet liquid temperature is 400°C. Figure 11 represents the liquid temperature and Figure 12 represents the liquid velocity in the bundle.

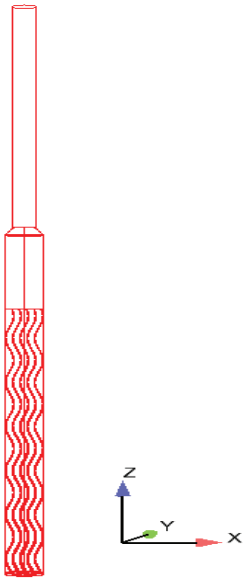

Figure 8: General view of the computational domain (length=2.31m) . Above the part where the fuel is located, it exists an adiabatic part (without fuel) with a large value of the hydraulic diameter.

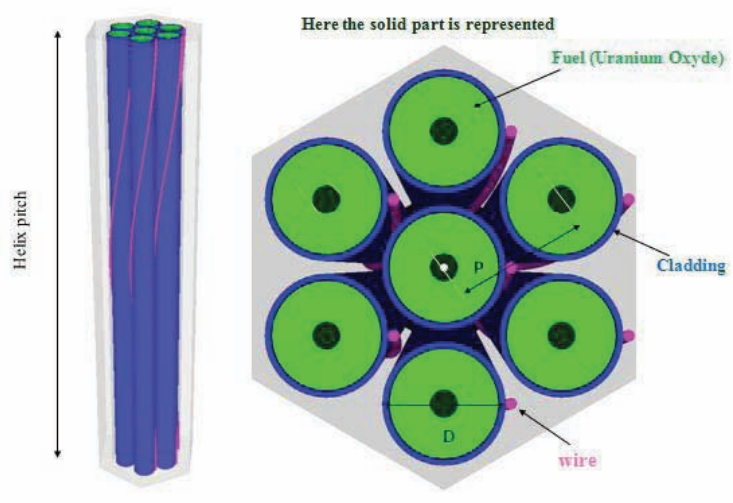

Figure 9: Geometry introducing the wrapped wire (limited in this view to one helix and only 7 pins).

The pitch-over-diameter ratio P/D and the helix-over-diameter ratio H/D is P/D=1.1 and H/D=21.

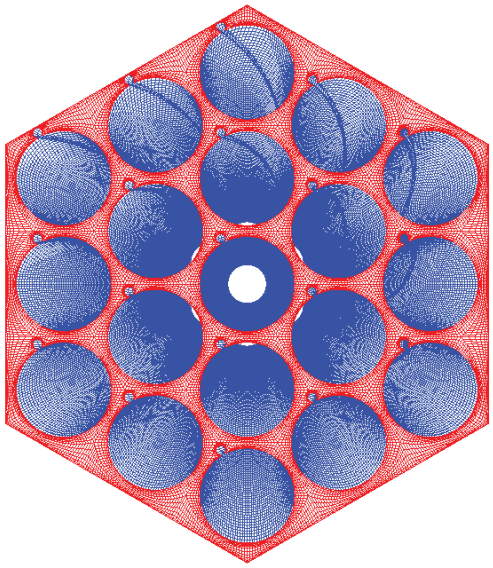

Figure 10: General view of the computational domain : about 4 Millions of cells for the fluid and 12 M of cells for the solid part.

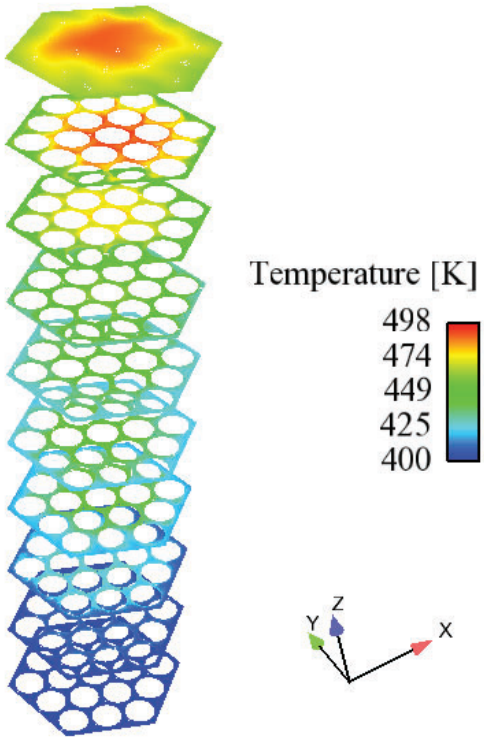

Figure 11: Liquid temperature

Computations show a pressure drop at the end of the heated length due to the sudden increase of the hydraulic diameter. Thus, the pressure can drop below the vapour pressure leading to liquid vaporization. This preliminary result supports the assumption of boiling in the upper subassembly zone (by autovaporization) which could possibly lead to a sodium boiling stabilization.

7. CONCLUSION

In order to evaluate the wall law implemented in the CFD tool, computations have been compared with KALLA experimental results obtained in the case of a rod heated with a constant heat flux which is concentrically embedded in a pipe liquid metal flow (single-phase flow).
Secondly, the incipient boiling superheat of sodium is quite different from that of conventional fluids. As a consequence, the nucleate boiling model has been improved and validated against the Charlety's experiment where a rod heated with a constant heat flux is concentrically embedded in a pipe sodium flow. For different values of the heat flux, the pressure is measured at different locations as function of the mass flow rate. A reasonable agreement has been reached which is very encouraging for further applications.
Finally, preliminary computations have been carried out in an assembly constituted of 19 pins equipped with a wrapped wire. Computations are qualitatively in accordance with the assumption of boiling in the upper subassembly zone which could possibly lead to a sodium boiling stabilization.

In further computations, numerical results will be compared to partial experimental results available in order to reproduce the internal characteristic and to exhibit a sodium boiling stabilization.

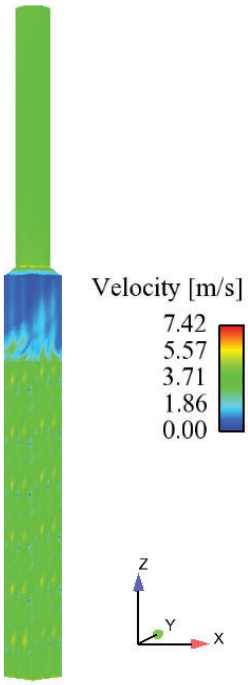

Figure 12: Liquid velocity

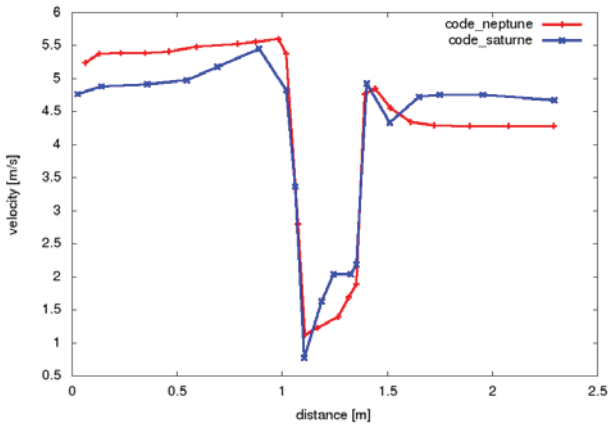

Figure 13: Axial profile of the liquid velocity. Comparison between Code_Saturne (developed by EDF R&D, the code is able to solve steady or transient, single phase, incompressible, laminar or turbulent flows) and Neptune_CFD

ACKNOWLEDGMENTS

The authors are grateful to the projects GEN IV (EDF) and NEPTUNE. The NEPTUNE project is funded by EDF (Electricité de France), CEA (Commissariat à l'Energie Atomique et aux Energies Alternatives), AREVA-NP and IRSN (Institut de Radioprotection et de Sûreté Nucléaire). The authors are grateful to C. Peniguel who has shared all the necessary inputs for the industrial application.

REFERENCES

1. J.M. Seiler, D. Juhel, Ph. Dufour "Sodium boiling stabilisation in a fast breeder subassembly during an unprotected loss of flow accident", Nuclear Engineering and Design 240 (2010) 3329–3335
2. N. Mechitoua., M. Boucker., J. Laviéville, J.-M. Hérard, S. Pigny, G. Serre, "An unstructured finite volume solver for two phase water/vapour flows based on an elliptic oriented fractional step method". Proceedings of the 10th Int. Topl. Mtg. Nuclear Reactor Thermal Hydraulics (NURETH 10), Seoul, Republic of Korea, (2003)
3. A. Guelfi, D. Bestion, M. Boucker, P. Boudier, P. Fillion, M. Grandotto, J.-M. Hérard, E. Hervieu, P. Péturaud, "NEPTUNE - A New Software Platform for Advanced Nuclear Thermal-Hydraulics", Nuclear Science and Engineering, 156, pp 281-324 (2007).
4. M. Ishii, « Thermo-fluid dynamic, theory of two phase », Eyrolles, collection de la direction des Etudes et recherches d'Electricité de France, 1975.
5. C.G. Speziale, S. Sarkar, and T.B. Gatski, "Modelling the pressure-strain correlation of turbulence: an invariant dynamical systems approach", 1991, J. Fluid Mech., pp. 227:245-272. ISSN 1469-7645.

6. S. Mimouni, F. Archambeau, M. Boucker, J. Lavieville, C. Morel, “A second order turbulence model based on a Reynolds Stress approach for two-phase boiling flow. Part 1 : Application to the ASU annular channel case”, Nuclear Engineering and Design, Volume 240, Issue 9, September 2010, Pages 2233-2243.
7. S. Mimouni, F. Archambeau, M. Boucker, J. Lavieville, C. Morel, “A second order turbulence model based on a Reynolds Stress approach for two-phase boiling flow and application to fuel assembly analysis”, Nuclear Engineering and Design, Volume 240, Issue 9, September 2010, Pages 2225-2232.
8. N. Zuber, M. Ishii “Drag coefficient and relative velocity in bubbly, droplet or particulate flows”, 1979, AIChE Journal, pp. 843-855.
9. N. Kurul and M.Z. Podowski, “Multidimensional effects in forced convection subcooled boiling”, Proceedings of the Ninth International Heat Transfer Conference Jerusalem, Israel, August (1990), pp. 21–26 (1990).
10. N. Zuber, “On the dispersed two-phase flow in the laminar flow regime”, Chem. Eng. Sc., No. 19, p. 897 (1964).
11. A. Tomiyama, et al “Transverse migration of single bubbles in simple shear flows”, 2002, Chem. Eng. Sci., pp. 1849-1858.
12. H.C. Unal, “Void fraction and incipient point of boiling during the subcooled nucleate flow boiling of water”, International Journal of Heat and Mass Transfer 20 (1977), 409-419.
13. B. Ramstorfer, H. Breitschadel, G. Steiner, “Modelling of the near-wall liquid velocity field in subcooled boiling flow”, Proceedings of the ASME Summer Heat Transfer Conference San Francisco, CA, July (2005) HT2005-72182 (2005).
14. A. Douce, S. Mimouni, M. Guingo, C. Morel, J. Laviéville, C. Baudry, “Validation of NEPTUNE_CFD 1.0.8 for adiabatic bubbly flow and boiling flow”, submitted to Nuclear Engineering and Design.
15. R. Stieglitz et al. “Heavy liquid metal technologies development in Kalla” 2006, Proceedings of ICAPP, Vol. Paper-id 6277.
16. “Handbook on Lead-Bismuth Eutectic Alloy and Lead, Properties, Materials, Compatibility, Thermalhydraulics and Technologies”. Report No. 6195, 2007, OECD-AEN/NEA.
17. P. Charlety, « Ebullition du sodium en convection forcée », Faculté des sciences de l'université de Grenoble : s.n., 1971. In french.
18. C. Péniguel, “Conjugate heat transfer study of a wire spacer SFR fuel assembly with the thermal code SYRTHES and the CFD code Code_Saturne”, ICAPP 2014 Charlotte, USA, April 6-9, 2014 Paper 14082.
19. B. Menant, “Nucleation, dry-out and boiling behind a sodium tight-local blockage in a 19-pin bundle with helical wire spacers”, Liquid metal boiling working group, 7th Meeting, Petten, 1-3 June 1977, (1977).